Int. J. Nanosci. Nanotechnol., Vol. 19, No. 1, March 2023, pp. 51-64
DOI: 10.22034/ijnn.2023.557273.2234

***Short Communication***

# Synthesis and Characterisation of Bimetallic Decorated with Graphene Oxide Nanocomposite as an Outstanding Adsorbent Material in the Removal of Methylene Blue

**K. Gayathri and Perumal Andal***

Research Scholar, School of Basic Sciences, Department of Chemistry, Vels Institute of Science Technology and Advanced Studies, Pallavarm, Kancheepuram, District Chennai - 600117, Tamil Nadu, India

(*) Corresponding author: andalprithu.sbs@velsuniv.ac.in
*(Received: 6 July 2022 and Accepted: 31 January 2023)*

***Abstract***

*Bulky nanocomposite materials in many miscellaneous technical domains, hybrid films, patterned structures, and core-shell particles are emerging as fascinating functional materials with features that go beyond the current state of the art. This section of Nanomaterials covers all aspects of nanocomposites, including design, synthesis, characterization, and application for a wide range of applications. Because of its poisonous nature, Methylene Blue (MB) dye, which is widely used in a variety of sectors, poses a hazard to the environment. Before being out into the location, wastewater from an assortment of businesses must be treated. As an adsorbent, we created a Zn-Cu-GO nanocomposite using a one-pot hydrothermal technique. The effect was related to Zn-Graphene Oxide and Cu-Graphene Oxide nanocomposites for the elimination of Methylene Blue colouring. The adsorption capacity of the Cu-GO, Zn-GO and Cu-Zn-GO nanocomposite were measured to be 308 mg $g^{-1}$ and 392 mg $g^{-1}$ and 544 mg $g^{-1}$, respectively. The removal efficiency of Cu-GO, Zn-GO and Cu-Zn-GO nanocomposite were recorded to be 72%, 82.3%, and 95%, respectively. The functional groups in the nanocomposite were also validated by the functional groups in the nanocomposite after the hexagonal Zinc nanoparticles and cubic Copper nanoparticles were examined using X-Ray diffraction (XRD). Fourier transform infrared (FT-IR) spectroscopy is a method. Both the flakes type Copper nanoparticle and the flakes type Zinc nanoparticle share a similar morphology. Granular copper nanoparticles were found on GO sheets and characterised by transmission electron microscopy.*

***Keywords:*** *Langmuir isotherm ($K_L$), Freundlich isotherm ($K_f$ ), Temkin isotherm ($K_T$), Copper (Cu), Zinc (zn), Graphene oxide (GO), Methylene Blue (MB).*

## 1. INRODUCTION

Nanotechnology speaks to the plan, creation and use of materials at atomic, molecular and macromolecular level, keeping in mind the end goal to deliver new nano-sized materials. As of late, the meeting of nanometer size scale advancements and biological techniques has paved way for the new field of Nano biotechnology. It is generally centred on the creation, control, and utilization of materials at the nanometer scale for cutting edge biotechnology [1].

Bimetallic nanoparticles, due to the synergistic effect produced when two different metals are mixed, bimetallic nanoparticles can display a range of features. This phenomenon can emphasise or expand their uses as antibacterial agents, drug delivery systems, and imaging agents by enhancing their characteristics and properties [2, 3]. Nanoparticles have a

range of potential applications in various fields' like medicine, environment, energy, electronics, manufacturing of material etc., [4-6].

Zinc Oxide nanoparticles are friendly in nature for human and animals, it is a strong antibacterial property which is used in less quantity is used in the absence in light and also it is most stable under any harsh conditions [7, 8]. Band gab 3.31eV, exciton energy of binding is 60 MeV, strong microbial, antibacterial property and also antifungal agent of Zinc oxide nanoparticles is low cost material too [8,9]. Using a small amount of Zinc oxide nanoparticles given an excellent interaction between bacteria due to their biostatic behaviour and also due their large surface area it is given an excellent in UV radiation blocking compared with bulk materials [10-14].

Since the severity of this pervasive issue is getting worse, environmental contamination has generated concern on a global scale, with a focus on water pollution [15, 16]. Despite the fact that antibiotics have significantly improved human health and longevity, those who drink contaminated water that contains antibiotic-resistant bacteria run the risk of developing superbugs that are untreatable. Additionally, wastewater discharged by factories producing textiles, leather, paper, printing, dyes, plastics, steel, and electroplating has a high concentration of heavy metals and organic dyes, harming the environment and ecosystem significantly [17, 18]. Environmental remediation has climbed to the top of the agenda and evolved into a significant study area as environmental worries about pollution and clean energy have grown. Environmental remediation has risen to the top of the debate and become a significant field of study as a result of new environmental concerns about pollution and clean energy. As a result of growing urbanisation and unsustainable population expansion, enormous volumes of organic pollutants have been discharged into the environment over the past few decades [19–22]. Nano material especially Zinc Oxide act a predominant role in cleaning of industrial effluents, it's having maximum potential to remove an industrial dye effluent [23-25].

## 2. EXPERIMENTAL

Graphene oxide is made up of graphene sheets primarily embellished with hydroxyl and epoxide groups. Due to the evaporation of the intercalated water and the evolution of gases from the pyrolysis of the oxygen-containing functional groups, rapid heating of GO causes expansion and delamination. The method of synthesis and level of oxidation have an impact on the structure and characteristics of GO. Hummer's method is the most widely used synthesis method in chemistry. The oxidising agents used to exfoliate the graphite flakes in this method of synthesis could be changed. Here, we show two synthesis techniques: the conventional method and the Hummer's method, which is a modified version of the conventional method. 200ml of H2SO4 was combined with 5g of graphite flakes and 2.6g of $NaNO_3$ in a 1000ml beaker. After stirring for an hour, 20g of $KMnO_4$ was gradually added, and they continued stirring continuously for 5 days. After 5 days, the solution's colour finally turned brown. To stop the reaction, which was detected by the appearance of yellow colour, 20ml of 30% $H_2O_2$ were added.200 ml of water were added to make a pure liquid that was yellowish. After allowing the mixture to settle, decanting three times, several washes, and centrifuging and filtering with 10% HCl before repeating the process several times with distilled water. After filtration, dry in a room with a vacuum. Using the Hummer method to prepare the graphite oxide, which was then sonicated in water to exfoliate it into graphene oxide.

These mono- and bimetallic nanoparticle catalysts on Go were made using a chemical reduction process. The first

catalyst, Cu-Go bimetallic NPs, was made by adding 0.06mm of copper sulphate to a 100ml round bottom flask along with zinc sulphate. After being sonicated for 30 minutes with 5 mg and 30 ml of water, GO was added to the mixture above, and the reaction was stirred for an additional 2 hours at 120 °C. Finally, the reaction mixture was diluted with 0.1M sodium borohydride solution. After cooling, the resulting solution was centrifuged at 2500 rpm. The ethanol and water used for additional purification. In a vacuum oven, the collected product was dried at 70°C. The preparation of Cu-Zn, Go, Cu, and Zn NPs, which are bimetallic and monometallic nanoparticle catalysts, followed a similar procedure and used the same quantity of reagents and experimental approach. $CuSO_4$ and $ZnSO_4.7H_2O$ solution served as the metal precursors for Cu-Zn, Go, Cu, and Zn nanoparticles. The alteration in colour revealed the decrease in Cu/Zn and GONPs. UV, SEM, and XRD analysis were used to characterise the two distinct bimetallic nanoparticle catalysts that were produced.

### 2.1. Synthesis of Zinc Decorated on Graphene Oxide Nanocomposite

Initially, the well-known modified Hummers' method was used to prepare GO. By sonicating 90.0 mg of GO for 5 hours in 90.0 ml of distilled water, a GO solution was created. The GO solution was next treated to the addition of zinc sulphate (30.0 mM) salt, which was continuously stirred for 15 minutes. The entire solution was subjected to hydrothermal treatment for 12 hours at a temperature of 180 °C. At the conclusion of the experiment, the precipitate was centrifuged three times through ethanol and water before being dried for 12 hours at 60 °C.

### 2.2. Synthesis of Copper Decorated on Graphene Oxide Nanocomposite

At the beginning, GO solution was made via sonication in a 1:1 ratio. After stirring for 30.0 minutes, 30.0 mM of copper sulphate was added to the solution. The entire solution was then subjected to a 12-hour hydrothermal treatment at 180 °C. Following a thorough washing of the precipitate, the sample was dried for 12 hours at 60 °C in order to collect the composite Cu-GO

### 2.3. Synthesis of Zinc and Copper Decorated on Graphene Oxide Nanocomposite

A solution of GO at a concentration of 1:1.20.0 ml of zinc sulphate (30.0 mM) and copper sulphate (30.0 mM) was produced under 5 hours of sonication. The solution was then combined with the GO solution for 30 minutes while being constantly stirred. The entire solution was placed in an autoclave and heated to 180 °C for 12 hours. Finally, the precipitates were separated and centrifuged three times in distilled water before being dried in a vacuum oven for 12 hours at 60 °C.

## 3. RESULT AND DISCUSSIONS

### 3.1. XRD

The diffractogram created for graphene oxide is displayed in Figure 1-3. It is possible to obtain a sharp diffraction peak at the start of the diffractogram by using the synthesis process to create a few layers of graphene. The newly found peak is associated with planes (002) that connect to carbon's HC structure. The leaves that are not arranged in monolayers have diffraction peaks visible in the diffractogram; monolayers do not have a diffraction peak visible. Because of this, in addition to the production method, it is also clear that the GO used in this inquiry has numerous levels. When compared to pure graphite, which is used to manufacture GO, demonstrates a reduction in the diffraction angle. This is owing to the presence of water molecules between the layers as well as an increase in GO interplanar lengths brought on by the insertion of functional groups during oxidation [26]. Figure 2 displays the

diffractograms for composite Cu/GO and pure copper powder, with the peaks corresponding to planes (111), (200), (220), (311), and (312). (222). No other peak was indexed, indicating that the copper powder did not contain any additional elements or oxidation or that the current oxidation produced only a small amount of oxide, insufficient to produce a peak above the diffractogram noise. These plans are specific to the FCC structure of copper. Furthermore, the concentration used to create the composite was so low that it failed to create a diffraction peak, hence there was no peak for the GO.

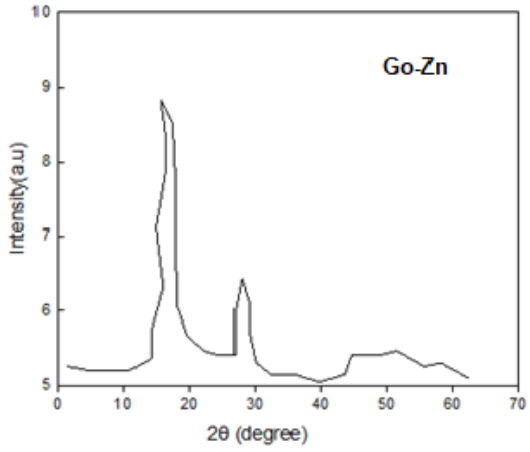


***Figure 1.****XRD images of GO-Zn.*

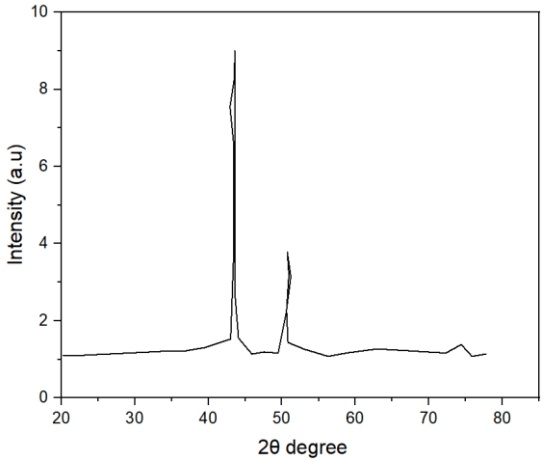


***Figure 2.****XRD images of GO-Cu.*

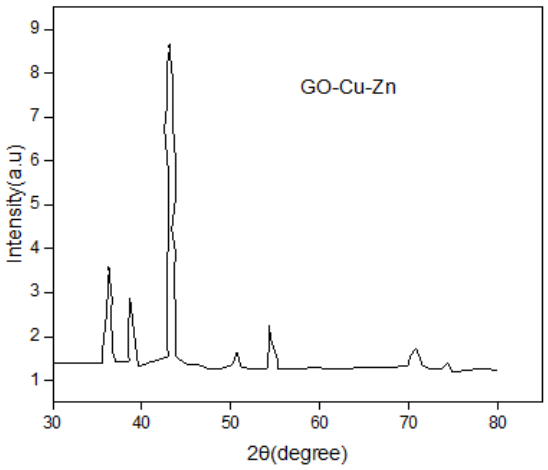


***Figure 3.****XRD images of GO-Cu-Zn.*

### 3.2. FESEM

FESEM analysis was used to look at the surface morphology of GO supported bimetallic alloy NPs. The surface morphology of Cu-Zn NPs supported by GO is shown in Figure 5. It is evident that GO supported the spherical shape of Cu–Zn NPs. Similarly, GO supported the spherical form of Cu-Zn NPs (Figure. 4-6). The bimetallic alloy NPs is well supported by GO based on the aforementioned findings.

### 3.3. FTIR

GO FTIR spectra Functional groups in GO that contain oxygen are present, as seen by the spectra as shown in the Figure.7-9. Peaks at 3300- $cm^{-1}$ to 3200- $cm^{-1}$ and 2127 $cm^{-1}$ display the stretching of the hydroxyl group, the carbonyl group at 1637 $cm^{-1}$, and the C-O epoxide group at 1190, 1177, and 1045 $cm^{-1}$, respectively. Large amounts of groups containing oxygen are present following the oxidation process, as indicated by the GO's main peaks' high intensities.

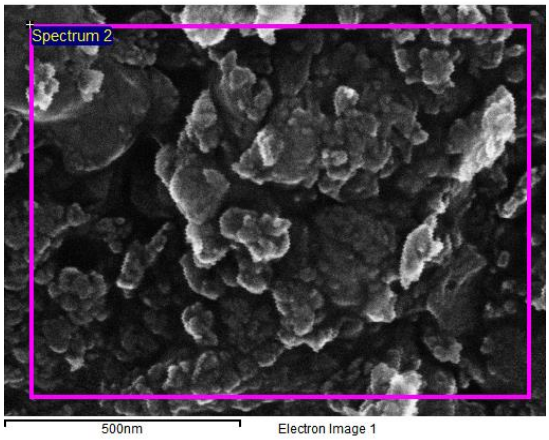


***Figure 4.*** *FESEM images of GO-Zn.*

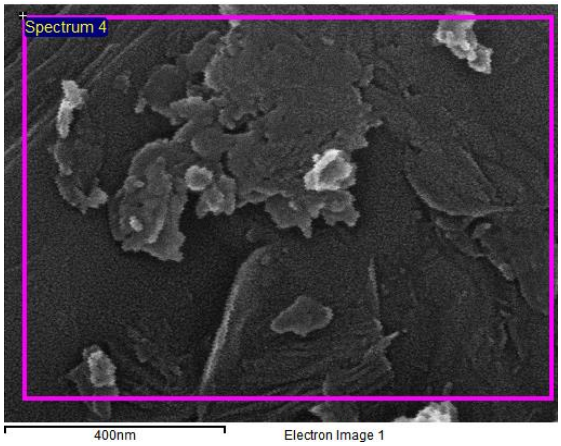


***Figure.*** *5 FESEM images of GO-Cu-Zn.*

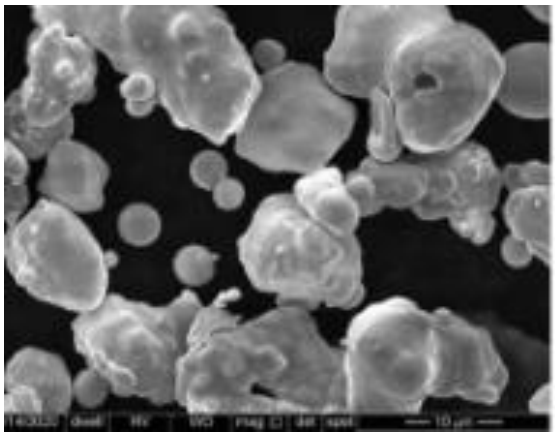

***Figure 6.*** *FESEM images of GO-Cu.*

The stretching of the alkene group's skeleton is what causes the peak at 1620 $cm^{-1}$. After GO peak intensities were reduced, there was phenol ring stretching at 1637 cm-1 and a considerable decrease in peak intensities attributable to alkoxy and hydroxyl groups.

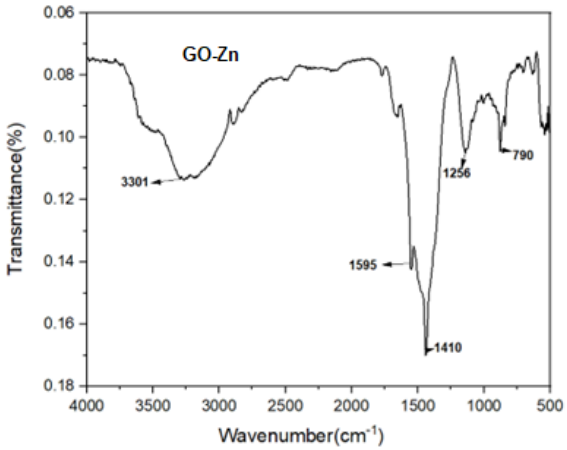


***Figure 7.*** *FTIR-GO-Zn.*

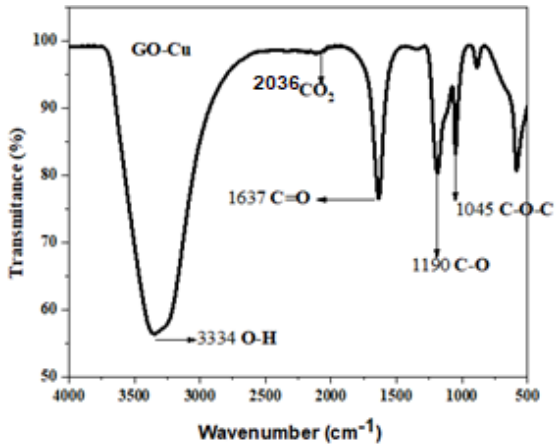


***Figure 8.*** *FTIR-GO-Cu.*

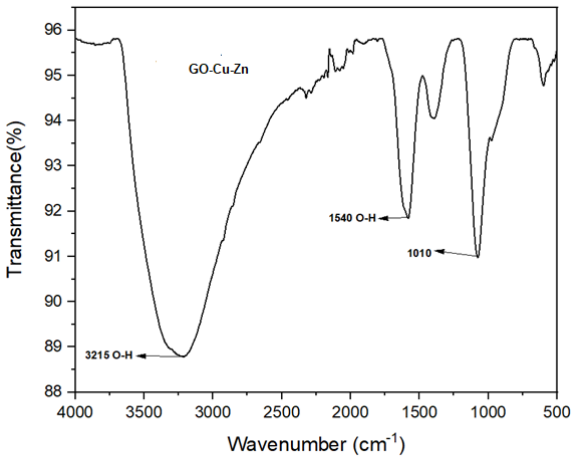


***Figure 9.*** *FTIR-GO-Cu-Zn.*

### 3.4. SEM

SEM analysis was used to determine the surface morphology of these three monometallic nanoparticle catalysts, and when the results were compared to the

equivalent polymer control, it was discovered that the surfaces were homogeneously smooth throughout. Contrarily, the Cu, and Zn NPs produced from Figure 10-12 show that a uniformly distributed white dot has emerged on the surface of mono metallic NPs, regardless of the photographs. This must be a result of the creation of NPs that are equally spaced over the surface of the spherical shape. Mono metal nanoparticles are highly supported by GO based on the findings.

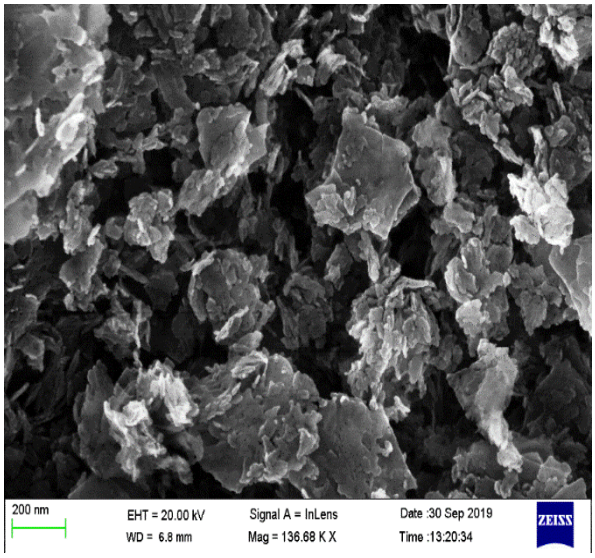


***Figure 10.****SEM image of GO-Zn.*

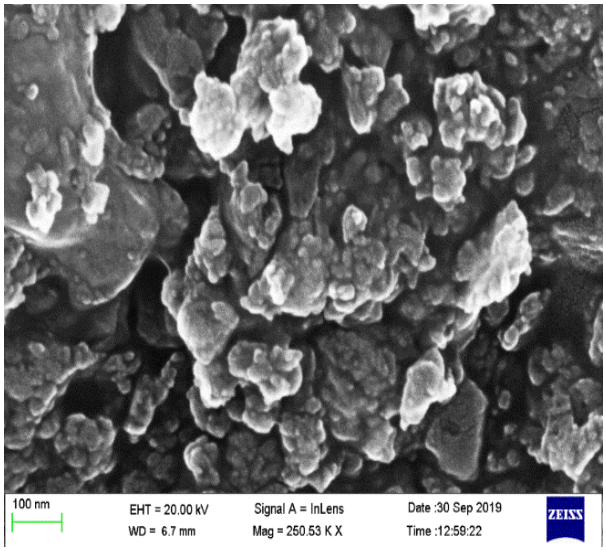


***Figure 11.*** *SEM image of GO- Cu.*

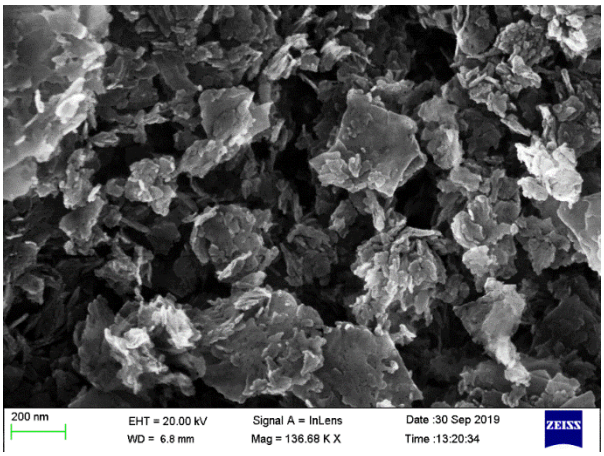


***Figure 12.****SEM image of GO- Cu-Zn.*

### 3.5. EDAX

EDAX analysis was used to calculate the weight fraction of Cu and Zn alloy NPs (Figure.13–16). The mono GO supported Zn NPs at 500nm comprise 72.49 weight percent of C, 25.29 weight percent of O, and 2.23 weight percent of Zn NPs, according to the EDAX measurement. 77.61 weight percent of C, 20.62 weight percent of O, and 1.77 weight percent of Zn NPs are present in this mono GO supported Zn NPs in 1 m.

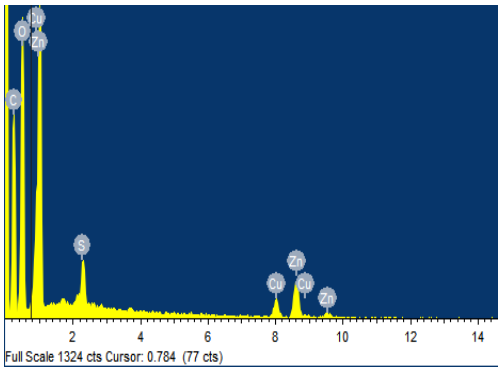


***Figure 13.*** *EDAX in Go-Zn-Cu nanoparticles (in 500nm).*

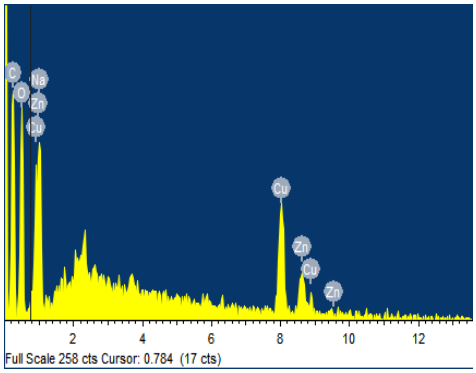

***Figure 14.*** *EDAX in Go-Cu-Zn nanoparticles (in 1µm).*

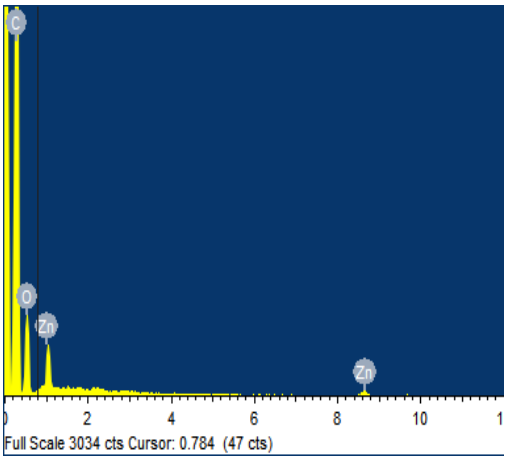


***Figure 15.*** *EDAX in Go-Zn-Cu NPS in 400n.*

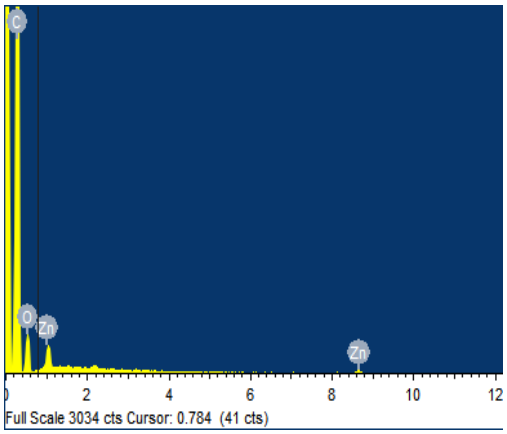


***Figure 16.*** *EDAX in Go-Zn-Cu NPS in 2nm.*

### 3.6. Compositional Analysis

By using EDAX [27-30] analysis, the elements in GO-Zn and Zn-doped materials were confirmed, and the EDX spectra are displayed in Figures 13 and 16. Three distinct peaks that correspond to C, O, and Zn are seen in Figs. 14 and 15, which supports the production of GO-Zn. For the GO-Zn NPs, the Go and Zn ratio in the EDX study is almost 100%. Table 1 demonstrates that as Zn concentrations rise, both the atomic percentage (at%) and mass percentage (mass%) of Zn drop. The maximum figure of Zn mass percentage, according to the EDAX report, is 2.23 for 0.45at percent Zn content. Zn doped GO NPs have a higher Zn mass percent content.

***Table 1.*** *EDX Weight ratio of Go-Zn nanoparticle.*

| *Sample GO-Zn* | Elements in atomic weight | | | Elements in mass weight | | |
|---|---|---|---|---|---|---|
| | C | O | Zn | C | O | Zn |
| *Spectrum 1* | 78.89 | 20.66 | 0.45 | 72.49 | 25.29 | 2.23 |
| *Spectrum 2* | 83.08 | 16.57 | 0.35 | 77.61 | 20.62 | 1.77 |

EDAX analysis was used to quantify the weight % of Cu and Zn alloy NPs (Figure.15 and 16). Bimetallic GO supported Zn and Cu NPs at 400 nm comprise 36.82 weight percent of C, 25.93 weight percent of O, 9.80 weight percent of Zn, and 23.25 weight percent of Cu NPs, according to the EDAX measurement. 37.24 wt percent of C, 44.08 wt percent of O, 4.33 wt percent of Zn, and 12.68 wt percent of CuNPs are present in the bimetallic GO supported Cu- Zn NPs in 1 m.

***Table 2.*** *EDX Weight ratio of Go-Zn-Cu nanoparticle.*

| *Sample GO-Zn-Cu* | Elements in atomic weight | | | | Elements in mass weight | | | |
|---|---|---|---|---|---|---|---|---|
| | C | O | Zn | Cu | C | O | Zn | Cu |
| *Spectrum 1* | 56.93 | 30.10 | 2.78 | 6.98 | 36.82 | 25.93 | 9.80 | 23.25 |
| *Spectrum 2* | 50.25 | 44.66 | 1.11 | 3.14 | 37.24 | 44.08 | 4.33 | 12.68 |

### 3.7. Compositional analysis:

The factors in GO-Zn-Cu [31] NPs have been showed via way of means of EDX evaluation and the EDX spectra are proven in Figure 15. and sixteen. In Figure 15. and sixteen suggests 4 robust peaks are found similar to C, O and Zn that confirms the formation of GO-Zn-Cu. The ratio of Go

and Zn in EDX evaluation is nearly 100 % for the GO-Zn-Cu NPs. Table 2 suggests that the atomic percent (at%) and mass percent (mass%) of Zn lower with the growth of Zn concentrations. EDAX document exhibits that the best cost of Cu mass percent is 23.25 for 6.98 at % of Cu awareness and the best cost of Zn Mass percent is 12.68 for 3.14 at% of Zn Concentration. The quantity in mass % of Cu and Zn is bigger in Cu-Zn doped GO NPs.

### 3.8. Anti-Microbial Activity for Graphene Oxide with Zinc and Copper

Samples were dissolved in alkyl group alcohol victimization extremist sonication for three hours. Medicament activity of solvent extracts decided by agar well diffusion method. Inoculant containing 106 cfu/ml of every bacterial culture was unfold on agar plates employing a sterile swab moistened with each bacterial suspension. Eight metric linear unit diameter wells were punched into the agar medium and loaded with one hundred µl (1 mg/ml) of answer and allowed to diffuse at area temperature. The take a look at plates were incubated in upright position for twenty-four h at 37° as shown in the Figure 17 and also in Table.3. Wells with identical volume plant product and water served as negative controls. After twelve hours incubation, the diameters of the inhibition zones were measured in mm.

***Table 3.*** *Anti-Microbial Activity for GO-Zn-Cu.*

| SI No | Pathogen detail | GO with Zinc | GO with Zinc and Copper | Control |
|---|---|---|---|---|
| 1 | ATCC 25922 | 35mm | 25mm | 0mm |
| 2 | ATCC 700603 | 15mm | 15mm | 8mm |
| 3 | MRSA | 21mm | 17mm | 0mm |
| 4 | ATCC 2146 | 22mm | 24mm | 13mm |
| 5 | ATCC 17802 | 14mm | 13mm | 13mm |

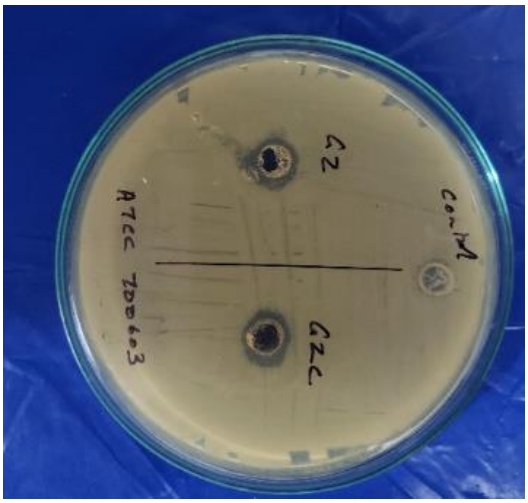


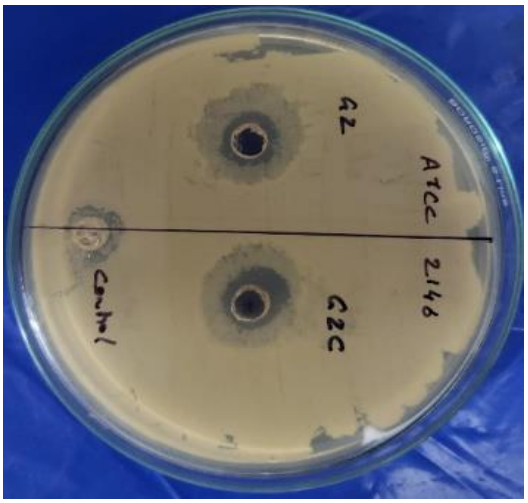

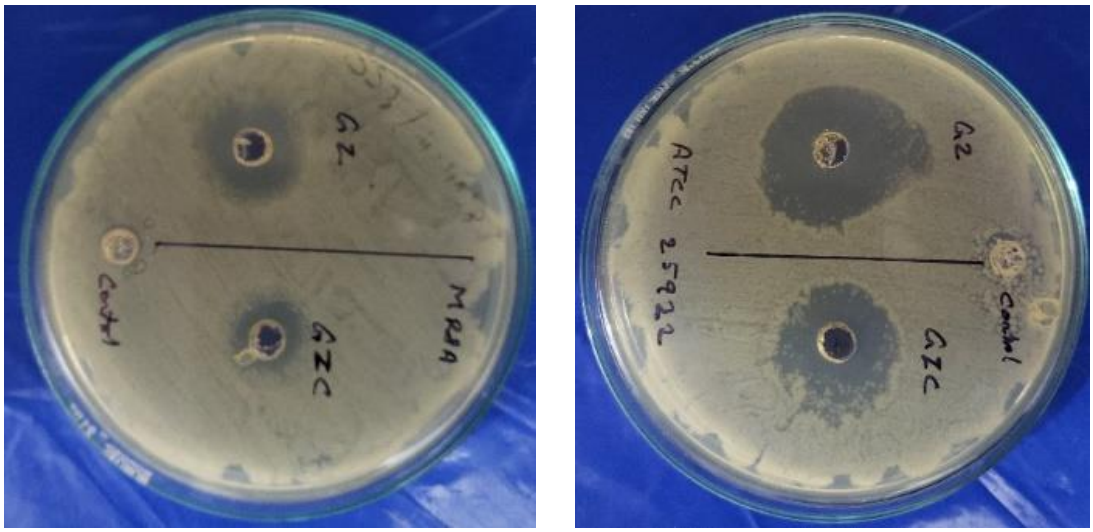


***Figure 17.*** *Anti-Microbial Activity for Graphene Oxide with Zinc and Copper.*

### 3.9. Adsorption Study

For this work, dye solutions at various concentrations were used. The dye solution's concentration ranges from 0-90 mg $L^{-1}$. Every parameter that was debated and optimised was fixed. The removal effectiveness of the Cu-GO, Zn-GO, and Cu-Zn-GO adsorbents at 0-90 mg $L^{-1}$ of MB dye solution is displayed in Figure 18. Cu-GO and Zn-GO nanocomposite were found to have removal efficiencies of 72% and 82.3 % respectively. The removal efficiency was raised to 95% when both metal nanoparticles were connected to the GO sheets (Cu-Zn-GO). As a result, the material Cu-Zn-GO functions as a superb adsorbent while removing MB dye. Figure 19. Displays the relationship between the adsorption capabilities of Cu-GO, Zn-GO, and Cu-Zn-GO adsorbents and the concentration of MB solution. Cu-GO was found to have an adsorption capacity of 308 mg $g^{-1}$, whereas Zn-GO nanocomposite had an adsorption capacity of 392 mg $g^{-1}$. The adsorption capacity of Cu-Zn-GO was discovered to be 544 mg $g^{-1}$, which is higher than that of Cu-GO and Zn-GO nanocomposite. Dye is bound to the surface of the nanocomposite due to an H-bond formed between the oxygen-containing groups in the Cu-Zn-GO nanocomposite and the nitrogen-containing groups in MB.

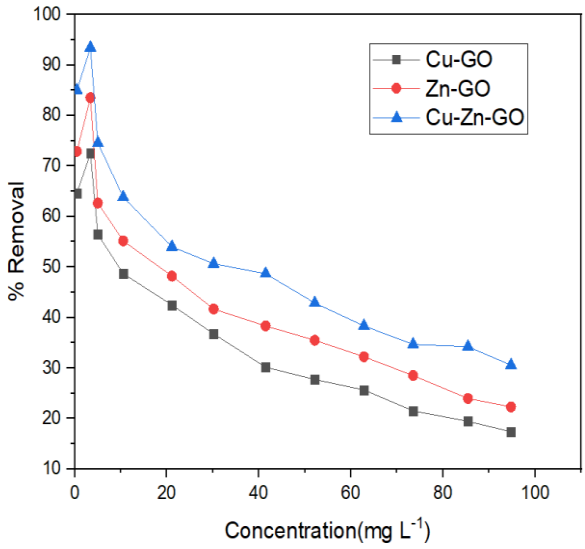


***Figure18.*** *Removal efficiency.*

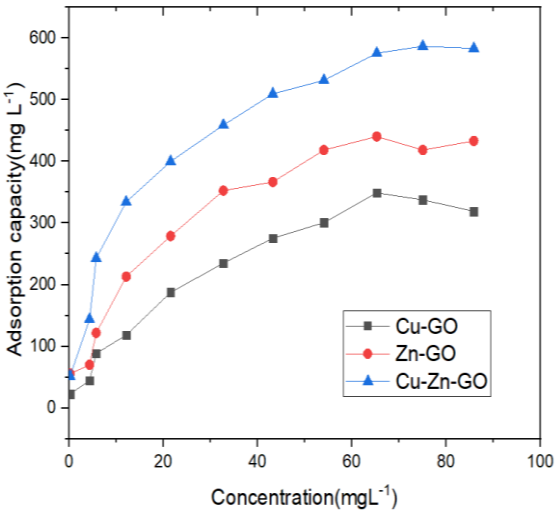


***Figure 19.*** *Adsorption capacity.*

The H-bond is strengthened and the adsorption sites on the GO surface are improved by the presence of two nanoparticles. We evaluated the Cu-Zn-GO [27, 28] nanocomposite's adsorption capability to that of other materials described in the literature, and the findings were better. The two metal nanoparticles, Cu and Zn, in the nanocomposite chemically and physically adsorb the alcohol molecule to its surface. The hydroxyl and carboxyl groups that can form a hydrogen bond with the MB dye molecules were previously achieved in the GO sheets. Again, the concentration of hydroxyl groups in the Cu-Zn-GO nanocomposite increases as a result of the hydroxylated surface of the metal nanoparticles. As a result, there are numerous active sites accessible for the adsorption of MB dye on the surface of Cu-Zn-GO nanocomposites. The amount of hydrogen bonds between the MB dye and the Cu-Zn-GO nanocomposite rises as a result. GO, Copper, and Zinc nanoparticles, which are all components of the nanocomposite, are thus involved in the adsorption of MB dye. Because there are more active sites present in Cu-Zn-GO nanocomposites, the adsorption process proceeds more quickly with greater removal efficiency.

### 3.10. Adsorption Isotherm

Adsorption isotherm studies are carried out to get qualitative data on adsorption capabilities and the distribution of adsorbate between the solid and liquid states. The Langmuir adsorption isotherm is one of three adsorption isotherms.

$$\frac{C}{q_e} = \frac{C}{q_m} + \frac{1}{q_m} K_L \qquad (1)$$

Freundlich Isotherm

$$\log q_e = \frac{1}{n} logC + logK_f \qquad (2)$$

Temkin Isotherm

$$q_e = BlnK_T + BlnC \qquad (3)$$

The equilibrium dye solution concentration, C (mg $L^{-1}$), is used in equations (1) through (3). The equilibrium amount of adsorbate on the adsorbent is represented by $q_e$(Equlibrium adsorbent). The Langmuir constant associated with adsorption energy is $K_L$(L $mg^{-1}$). The maximal adsorption capacity ($q_m$) of the adsorbent, which corresponds to total monolayer coverage, is $q_m$ (mg $g^{-1}$). The Freundlich constant for adsorption intensity is 1/n, whereas the Freundlich constant for adsorption capacity is $K_f$(L mg1). The Temkin isotherm binding constant ($K_T$ (L $g^{-1}$) and the heat of adsorption constant [B] are both constants. The calculations for the three adsorption isotherm equations (3) were followed by the calculations for the Cu, Zn, and GO adsorbents, which are fitted to all three equations (Figure 20–22). The calculated values are shown in Table 4, and it was discovered that the Langmuir isotherm was better suited to the calculation obtained from the adsorbents Fig. 20. With a $K_L$ value of 9.20 mg $L^{-1}$ and a maximum adsorption capacity (qm) of 640.88 mg $g^{-1}$, the regression ratio ($R^2$) for the Langmuir model (Fig.20) was determined to be 0.99. Similar computations were made for the Freundlich (Figure 21.) and Temkin isotherms (Figure 22.), both of which have regression ratios that are lower than the Langmuir isotherm. As a result, the adsorption process adheres to the Langmuir isotherm.

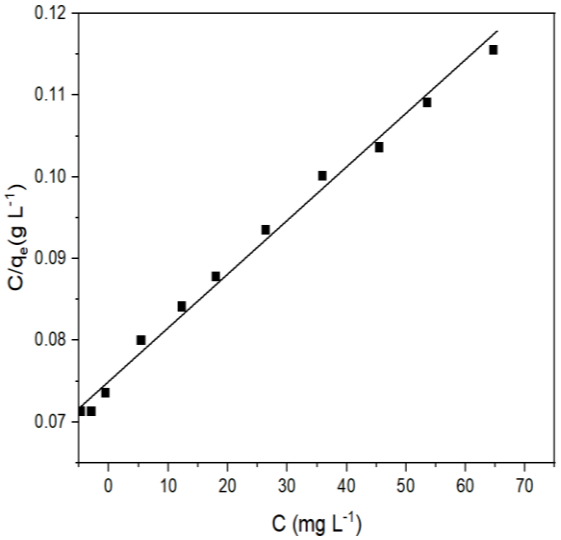


***Figure 20.*** *Langmuir Isotherm.*

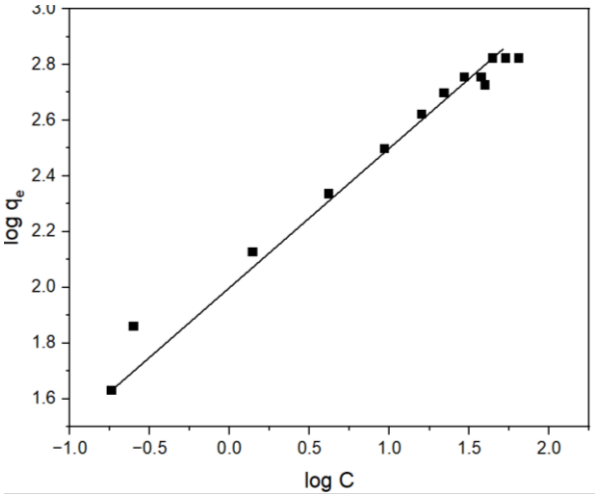


***Figure 21.*** *Freundlich Isotherm.*

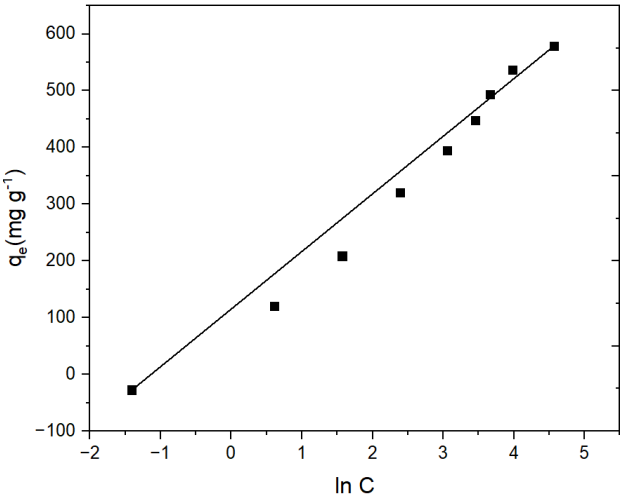


***Figure 22.*** *Temkin Isotherm.*

***Table 4.*** *Adsorption isotherms.*

| Adsorption material | Langmuir isotherm | | | Freundlich isotherm | | | Temkin isotherm | | |
|---|---|---|---|---|---|---|---|---|---|
| | $K_L$ (L $mg^{-1}$) | $q_m$ (mg $g^{-1}$) | $R^2$ | $K_f$ (L $mg^{-1}$) | n | $R^2$ | $K_T$ (L $mg^{-1}$) | B | $R^2$ |
| **Cu-Zn-GO** | 9.20 | 640.88 | 0.99 | 93.76 | 2.11 | 0.96 | 6.75 | 89.21 | 0.92 |

### 3.11. Adsorption Kinetics

To investigate the adsorption mechanism, four kinetic models are used, with the potential rate controlling steps being chemical reaction, mass transfer, and diffusion control.

Pseudo-first-order kinetic model is one of them.

$$\log(q_e - q_t) = \log q_e - \frac{K_1}{2.303} \times t \quad (4)$$

$q_e$ and $q_t$ represents the adsorption capacities at equilibrium and at time, $K_1$ Pseudo First order kinetics

Pseudo-second order kinetic model

$$\frac{t}{q_t} = \frac{1}{K_2 q_e^2} + \frac{1}{q_e} \times t \quad (5)$$

Intra particle diffusion mode

$$q_t = K_{id} \times t^{1/2} + C \quad (6)$$

Elovich model

$$q_t = \frac{1}{\beta}\ln(\alpha\beta) + \frac{1}{\beta}\ln t \quad (7)$$

The $q_e$ and $q_t$ (mg $g^{-1}$) are, respectively, the adsorption capacities at equilibrium and at a time 't' in equations (4)– (7). The pseudo-first-order kinetic model's rate constant is $K_1$ ($min^{-1}$), and the pseudo-second-order kinetic model's rate constant is $K_2$ (g $min^{-1}$). The intra-particle diffusion rate constant is known as $K_{id}$ (mg $g^{-1}min^{-1/2}$). In the Elovich model, " is the initial adsorption rate (mg $g^{-1}$ $min^{-1}$) and " is the desorption constant. A calculation relating to the adsorption kinetics was made, and the results are presented in Table 5 as a linear fit. With a regression ratio of 0.97 displays the linear fitting plot for pseudo-first-order kinetics (Figure 23.). The regression ratio was again found as 0.99 in the pseudo-second-order kinetic model shown in (Figure 24.), which is comparable to first-order kinetics [26]. The rate constants for the pseudo-second-order kinetic model ($K_2$) and adsorption capacity ($q_e$) were calculated from the linear fitting and were found to be $1.9 \times 10^{-3}$ g $mg^{-1}min^{-1}$ and 65.3 mg $g^{-1}$, respectively. Similar to this, the linear fitting for the Elovich model in Fig. 26 and the intraparticle diffusion model in Fig. 25 was carried out with regression ratios of 0.95 and 0.92, respectively. It's interesting to note that the linear fitting plots for the Intra-particle Diffusion Model (Figure 25.) and the Elovich Model (Figure 26.) are similar.

Although the adsorption capacity for the first order (26.34 mg $g^{-1}$) is lower than that of the second order kinetics (65.3 mg $g^{-1}$), the regression ratio value for both the pseudo-first order and pseudo-second order kinetic models is the same in this case. Pseudo-second-order kinetics is used here to govern the adsorption process.

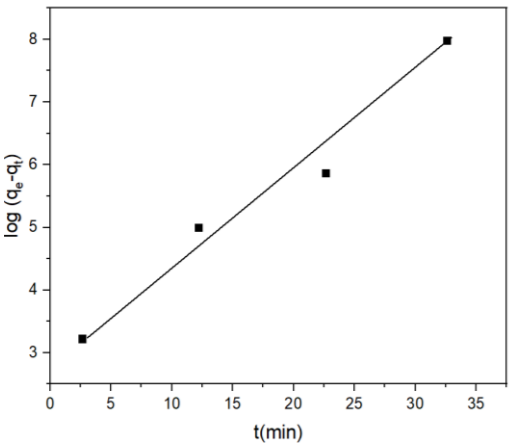


***Figure 23.*** *Pseudo first order kinetic.*

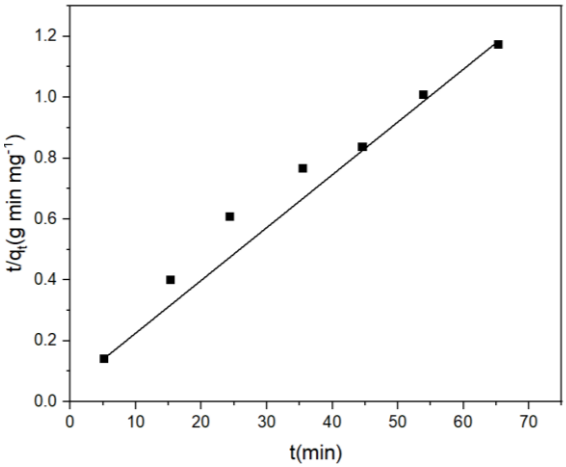


***Figure 24.*** *Pseudo Second order kinetic.*

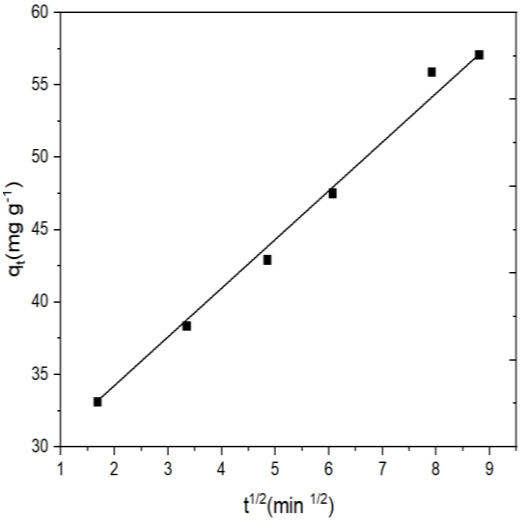


***Figure*** 25. *Intra particle diffusion model.*

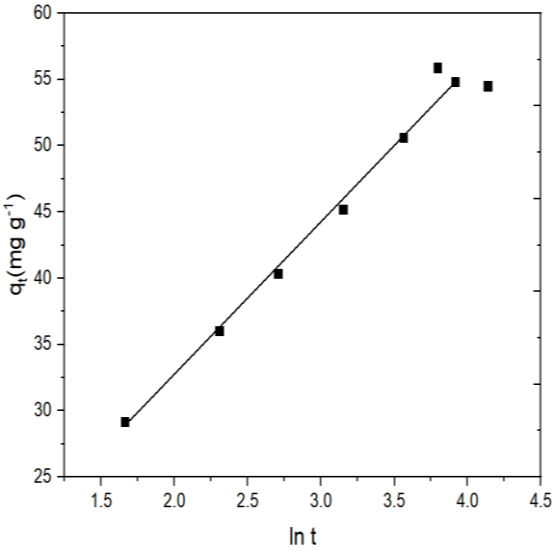


***Figure 26****. Elovich model.*

***Table 4.*** *Adsorption isotherms.*

| Adsorption material | Pseudo first order | | | Pseud second order | | | Intraparticle diffusion | | Elovich model | | |
|---|---|---|---|---|---|---|---|---|---|---|---|
| | $K_1$ (L $mg^{-1}$) | $q_e$ (mg $g^{-1}$) | $R^2$ | $K_2$ (g $mg^{-1}min^{-1}$) | $q_e$ | $R^2$ | $K_{id}$ (mg $g^{-1}$ $min^{-1/2}$) | $R^2$ | $\alpha$ (mg $g^{-1}$ $min^{-1/2}$) | $\beta$ ( g $mg^{-1}$ ) | $R^2$ |
| **Cu-Zn-GO** | 0.031 | 26.34 | 0.99 | $1.9\times10^{-3}$ | 65.3 | 0.96 | 5.10 | 0.95 | 38.42 | 0.10 | 0.92 |

## 4. CONCLUSION

The adsorbent Cu-Zn-GO was synthesized via the one-pot hydrothermal method and sent for the removal of MB dye. Two catalysts made of monometallic Cu and Zn and bimetallic Cu/Zn nanoparticles were supported by various types of graphene oxide. By co-reducing $NaBH_4$ in an aqueous medium, mono and bimetallic nanoparticles supported on graphene oxide were created. Using various methods, including scanning electron microscopy (SEM), X-ray diffraction spectroscopy, the obtained mono and bimetallic nanoparticle catalysts' shape and size were characterised (XRD). According to the results, newly developed graphene oxide supported bimetallic nanoparticle catalysts can be more effective at oxidising, reducing, and removing important organic pollutants from the environment. They are also excellent biologically active compounds. The composite was sent for the removal of methyl blue dye, owing to is excellent adsorbing capacity. In an optimized temperature, the adsorption experiment was conducted. The adsorption capacity and removal efficiency of Cu-Zn-GO nanocomposite were calculated to be 546 mg $g^{-1}$ and 96%, respectively which were greater than that of Cu-GO (378 mg $g^{-1}$ and 78%) and Zn-GO (394 mg $g^{-1}$ and 81.9%) nanocomposites. The adsorption process involved in the removal of MB dye follows the Langmuir isotherm and pseudo-second-order kinetics model.


## ACKNOWLEDGEMENT

The authors thank VISTAS for providing facilities to perform the work


## CONFLICT OF INTEREST

The author declares that there is no conflict of interests regarding the publication of this article.

## REFERENCES


1. Jaison, J., Ahmed, B., Yen, S. C., Alain, D., Michael K. D., "Review on nanoparticles and nanostructured materials: history, sources, toxicity and regulations", *Beilst. J Nanotechnol*., 9 (2018) 1050-1074 .
2. Medina-Cruz, D., "Bimetallic Nanoparticles for Biomedical Applications", A Review in Racing for the Surface, (2020) 397-434.
3. Padilla-Cruz, A. L., Garza-Cervantes, J. A., Vasto-Anzaldo, X. G., Gerardo García, R., Leon B.A., Morones-Ramírez, J. R., "Synthesis and design of Ag–Fe bimetallic nanoparticles as antimicrobial synergistic combination therapies against clinically relevant pathogens", *Nature*, 11(2021) 5351.
4. Ibrahim, K., Khalid, S., Idrees, K., "Nanoparticles: Properties, applications and toxicities", *Arab. J. Chem*., 12 (2019) 908-931.
5. Barrak, H., Saied, T., Chevallier, P., Laroche, G., Mnif, A., Hamzaoui, A. H., "Synthesis, characterization, and functionalization of ZnO nanoparticles by N-(trimethoxysilylpropyl) ethylenediamine triacetic acid (TMSEDTA): Investigation of the interactions between Phloroglucinol and ZnO@ TMSEDTA", *Arab. J. Chem*., 12 (2019) 4340-4347.
6. A.l-Heniti, S., Badran, R.I., Umar, A., Al-Ghamdi, A., Kim, S. H., Al-Marzouki, F., "Temperature dependent structural and electrical properties of ZnO nanowire networks", *Int. J. Nanosci. Nanotechnol*., 11 (2011) 1-7.
7. Pal, S., Mondal, S., Maity, J., Mukherjee, R., "Synthesis and Characterization of ZnO Nanoparticles using Moringa Oleifera Leaf Extract: Investigation of Photocatalytic and Antibacterial Activity", *Int. J. Nanosci. Nanotechnol*., 14 (2018) 111-119.
8. Zvekic, D., Srdic V. V., Karaman, M. A., Matavulj, M. N., "Processing and Application of Ceramics,"Development of silane grafted ZnO core shell nanoparticles loaded diglycidyl epoxy nanocomposites film for antimicrobial applications", *Materials Science and Engineering C*., 64 (2016) 260-292.
9. C. Guo., Z. Zheng., Q. Zhu., X. Wang., "Polyurethane/Zinc Oxide (PU/ZnO) Composite—Synthesis, Protective Property and Application", Center of Research Excellence in Corrosion, King Fahd University of Petroleum and Minerals, Dhahran 31261, Saudi Arabia. *Polymers*, 12(2020) 1535.
10. R. H., Wang., J. H., Xin., X. M., Tao W. A., Daoud., "ZnO Nanorods Grown on Cotton Fabrics at Low Temperature", *Chemical Physics Letters*, 398 (2004) 250-255.
11. R. H., Wang, J. H., Xin, X. M., Tao, "UV-blocking property of dumbbell-shaped ZnO crystallites on cotton fabrics", *Inorg. Chem*, 44 (2005) 3926-3930

12. R. K., Dutta, P. K., Sharma, A. C., Pandey, Dig. J. Nanomater., “Biomedical Applications of Silver Nanoparticles: An Up-to-Date Overview” *Nanomaterials*. 8 (2018) 681-706.
13. Vigneshwaran, N., Kumar, S., Kathe, A.A., Varadarajan, P.V., Prasad, “Functional Finishing of Cotton Fabrics Using Zinc Oxide-Soluble Starch Nanocomposites” *Nanotechnology*. 17(2006) 5087.
14. Yadav, A., Prasad, V., Kathe, A. A., “Functional finishing in cotton fabrics using zinc oxide nanoparticles”, *Bull Mater Sci* .**29**(2006) 641–645.
15. Husain, S., Verma, S. K., Yasin, D., Hemlata Rizvi, M. M. A., Fatma, T., “Facile green bio-fabricated silver nanoparticles from Microchaete infer dose-dependent antioxidant and anti-proliferative activity to mediate cellular apoptosis”, *Bioorg Chem.*, 107 (2021) 104535.
16. Khandual, A., Rout, N., Verma, S. K., Patel, P., Pattanaik, P., Luximon, Y., “Controlled nano-particle dyeing of cotton can ensure low cytotoxicity risk with multi-functional property enhancement”, *Mater Today Chem*., 17 (2020) 100345.
17. Santhosh, C., Daneshvar, E., Tripathi, K. M., Baltrenas, P., Kim T., Baltrenaite, E., “Synthesis and characterization of magnetic biochar adsorbents for the removal of Cr(VI) and Acid orange 7 dye from aqueous solution”, *Environ Sci Poll Res*., 27 (2020) 32874-32887.
18. Xia, W., Mahmood, A., Zou, R. Q., “Metal-organic frameworks and their derived nanostructures for electrochemical energy storage and conversion”, *Energy. Environ. Sci*., 8 (2015) 1837-1866.
19. Zhang, P., Gong, J. L., Zeng, G. M., Song, B., Fang, S., Zhang, M., “Enhanced permeability of rGO/S-GO layered membranes with tunable inter-structure for effective rejection of salts and dyes”, *Purif. Technol.*, 220 (2019) 309-319.
20. Shukla, S., Khan, I., Bajpai, V. K., Lee, H., Kim, T., Upadhyay, A., “Sustainable Graphene Aerogel as an Ecofriendly Cell Growth Promoter and Highly Efficient Adsorbent for Histamine from Red Wine”, *ACS. Appl. Mater Inter*., 11 (2019) 18165-18177.
21. Husain, S., Verma, S. K., Hemlata, A. M., Sardar, M., Haq, Q. M. R., Fatma, T., “Antibacterial efficacy of facile cyanobacterial silver nanoparticles inferred by antioxidant mechanism”, *Mater Sci & Eng C-Mater Bio Apps.*, 122 (2021) 1-10.
22. Abdi, S., Nasiri, M., “Enhanced hydrophilicity and water flux of poly (ether sulfone) membranes in the presence of aluminum fumarate metal-organic framework nanoparticles: preparation and characterization”, *ACS. Appl. Mater Interfaces*, 11 (2019) 15060-15070.
23. Banisharif, A., Hakim, E. S., Anaraki Firooz, A., Khodadad,I, A., Mortazavi, Y., “TiO2/Fe3O4 Nanocomposite Photocatalysts for Enhanced Photo-Decolorization of Congo Red Dye”, *Int. J. Nanosci. Nanotechnol.*, 9 (2013) 193-202.
24. Khan, R. S., Pathak, B., Fulekar, M., “Spherical Surfaced Magnetic (Fe3O4) Nanoparticles as Nano Adsorbent Material for Treatment of Industrial Dye Effluents”, *Int. J. Nanosci. Nanotechnol*., 13 (2017) 169-175.
25. Divya, B., Karthikeyan, C. H., Rajasimman, M., “Chemical Synthesis of Zinc Oxide Nanoparticles and Its Application of Dye Decolourization”, *Int. J. Nanosci. Nanotechnol*., 14 (2018) 267-275.
26. Hwang, J., Yoon, T., Jin, S.H., Lee J., Kim, T. S., Hong, S. H., Jeon S., “Enhanced mechanical properties of graphene/copper nanocomposites using a molecular-level mixing process”, *Ad. Mater.*, 25 (2013) 6724-6729.
27. Trupti, R. D., Prashant K. S., “Bimetal oxide decorated graphene oxide (Gd2O3/Bi2O3@GO) nanocomposite as an excellent adsorbent in the removal of methyl orange dye”, *Mate Sci. Semiconductor, Proc*., 105 (2020) 1-10.
28. Faria, G. S., Lima, A. M., Pinheiro, W. A., Ribeiro, A. A., Brandão, L. P. M., “copper-graphene composites produced by cold die compactation of powder metallurgy”, *São Paulo, Brazil*, 72 (2017) 2553-2560.
29. Isaque Alan de, B. M., Talita Gama, D. S., Andreza, M. L., Wesley Oliveira, D. S and Luiz, P. B., “Synthesis and Characterization of Graphene-Oxide Reinforced Copper Matrix Composite”, *Mater Proc* 4 (2021) 1-7.
30. Fatima, T. J., Woo-Gwang, J. J., Wook, L., “Facile and safe graphene preparation on solution based platform J of Indu”, *Eng. Chem.*, 20 (2014) 2883-2887.
31. Zuzanna, B., Marta, M. P., Stanisław, G., Łukasz, M., “Production and Properties of Molybdenum Disulfide/Graphene Oxide Hybrid Nanostructures for Catalytic Applications”, *Nanomaterials*, 10 (2020) 1-15.